Inorganic Chemistry

Article

pubs.acs.org/IC

Identifying a Structural Preference in Reduced Rare-Earth Metal Halides by Combining Experimental and Computational Techniques

Simon Steinberg,[†] Jakoah Brgoch,[‡] Gordon J. Miller,*[,‡] and Gerd Meyer[†]

[†]Department of Inorganic Chemistry, University of Cologne, Greinstraße 6, 50939 Cologne, Germany

[‡]Department of Chemistry, Iowa State University, Ames, Iowa 50011, United States

Supporting Information

ABSTRACT: The structures of two new cubic $\{TnLa_3\}Br_3$ (Tn = Ru, Ir; $I4_132$, $Z = 8$; Tn = Ru: $a = 12.1247(16)$ Å, $V = 1782.4(4)$ Å^3; Tn = Ir: $a = 12.1738(19)$ Å, $V = 1804.2(5)$ Å^3) compounds belonging to a family of reduced rare-earth metal halides were determined by single-crystal X-ray diffraction. Interestingly, the isoelectronic compound $\{RuLa_3\}I_3$ crystallizes in the monoclinic modification of the $\{TnR_3\}X_3$ family, while $\{IrLa_3\}I_3$ was found to be isomorphous with cubic $\{PtPr_3\}I_3$. Using electronic structure calculations, a pseudogap was identified at the Fermi level of $\{IrLa_3\}Br_3$ in the new cubic structure. Additionally, the structure attempts to optimize (chemical) bonding as determined through the crystal orbital Hamilton populations (COHP) curves. The Fermi level of the isostructural $\{RuLa_3\}Br_3$ falls below the pseudogap, yet the cubic structure is still formed. In this context, a close inspection of the distinct bond frequencies reveals the subtleness of the structure determining factors.

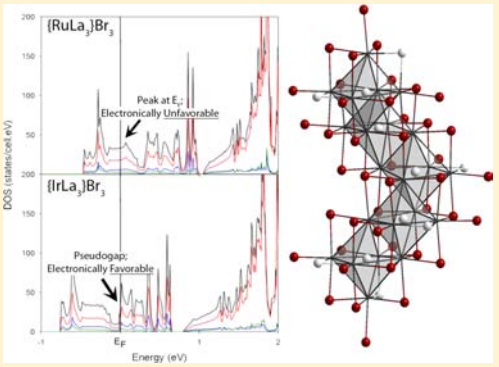

I. INTRODUCTION

Numerous rare-earth metal cluster halides have been observed adopting various structure types.[1] Most of these structures are composed of single or condensed cluster units that are centered by an endohedral atom.[1−6] These interstitially centered cluster units can be described as anti-*Werner* complexes because they are arranged in contrast to *Werner*'s classical concept as applied to solids.[7,8] In anti-*Werner* compounds, the interstitial atoms will have a higher electron affinity than their surrounding ligands, as seen, for instance, in the compound $\{Ir_4Y_{16}\}Cl_{24}$. Here, the central Ir atom has a higher electron affinity than the coordinated yttrium atoms that surround it. The yttrium atoms are also encapsulated by chloride atoms, which clearly have a higher electron affinity than yttrium.[6]

Another type of anti-*Werner* complex that reveals an interesting structural chemistry belongs to the broader family of $\{TnR_3\}X_3$-type structures, where Tn is a transition metal, R is a rare earth element, and X is a halogen.[9−15] These compounds show an exceptional range of structural diversity and chemistry, which involve interstitially centered, condensed R element clusters, while maintaining the same overall composition. In particular, five different structure types of the $\{TnR_3\}X_3$-family have been reported thus far: (1) a cubic $\{PtPr_3\}I_3$-type ($I4_132$),[9,10] (2) a tetragonal $\{NiLa_3\}Br_3$-type ($I4_122$),[11] two independent monoclinic structure types, (3) $\{RuPr_3\}I_3$-type ($P2_1/m$) and (4) $\{IrY_3\}I_3$-type ($P2_1/m$),[10,12−14] and (5) an orthorhombic $\{RuPr_3\}Cl_3$-type ($Pnma$)[15] structure. When R is La or Pr and X is Br or I, the cubic $\{PtPr_3\}I_3$-type as well as the monoclinic $\{RuPr_3\}I_3$-type will tend to crystallize.[9,10,12−14] Changing the R atom to late rare earth elements, that is, R = Gd or Er, results in the monoclinic $\{IrY_3\}I_3$-type structure, while the orthorhombic $\{RuPr_3\}Cl_3$-type will be obtained for early rare earths (R = Pr, Ce) and X = Cl.[14−16] Additionally, the endohedral transition metal (Tn) atoms can be substituted by a nonmetal or a semimetal from the third, fourth, or fifth main group.[17] These substitutions result in distortions of the clusters by decreasing their symmetry and prove that a large number of atoms can be incorporated into a cluster.[17] Such a wide range of compositions with varying structure types provides an alluring system to study composition-structure-bonding relationships.

Recently, the electronic structures of three different examples among the $\{TnR_3\}X_3$ compounds were investigated: (i) monoclinic $\{RuPr_3\}I_3$, (ii) monoclinic $\{MnGd_3\}I_3$, which adopts of the other monoclinic $\{IrY_3\}I_3$-type; and (iii) orthorhombic $\{RuPr_3\}Cl_3$. The various interatomic overlap populations, using COHP curves, and densities of states (DOS) for each of these structures were analyzed, and revealed different chemical bonding networks in these three cases.[18] For instance, using integrated COHP (ICOHP) values weighted by bond frequencies in the different structures, the relative contributions of heteroatomic Tn−R and R−X interactions to homoatomic Tn−Tn and R−R interactions increases from 73.5%:26.5% in $\{MnGd_3\}I_3$ to 82.5%:17.5% in $\{RuPr_3\}Cl_3$ to 91.0%:9.0% in $\{RuPr_3\}I_3$.[18] Although these three structures were analyzed based on a complex bonding network, conclusive evidence accounting for the structural changes was not

Received: April 23, 2012
Published: October 5, 2012

presented. Additional research on the electronic structure of a tetragonal $\{NiLa_3\}Br_3$-type structure was also analyzed using extended Hückel theory (EH).[11] The tetragonal structure is derived from the cubic $\{PtPr_3\}I_3$-type structure; however, a Jahn−Teller like structural distortion occurs because of the presence of Ni. The field strength of the interstitial Ni atoms on the La 5d orbitals leads to an uneven occupancy of the cluster t_{1u}-like orbitals, which results in the structural distortion. Although these investigations have interpreted the electronic structures of four out of the five known structure types with the general composition $\{TnR_3\}X_3$, to the best of our knowledge, electronic structure calculations on the cubic $\{PtPr_3\}I_3$-type have yet to be analyzed.

Therefore, we present the structural results and theoretical considerations on the electronic structures of the novel compounds $\{TnLa_3\}Br_3$ (Tn = Ru, Ir), which belong to the cubic family of the $\{TnR_3\}X_3$ type structures. In addition, the results obtained from crystal orbital Hamilton population (COHP) analysis are compared to the band structure of the known isoelectronic compound $\{TnLa_3\}I_3$ (Tn = Ru).[12,14] A comparison of the two structures provides justification of why a structural change exists between the $\{RuLa_3\}Br_3$ (cubic, $\{PtPr_3\}I_3$-type) and $\{RuLa_3\}I_3$ (monoclinic, $\{RuPr_3\}I_3$-type) compounds, but not in the $\{IrLa_3\}Br_3$ ($\{PtPr_3\}I_3$-type) and $\{IrLa_3\}I_3$ ($\{PtPr_3\}I_3$-type) systems.[9]

II. EXPERIMENTAL TECHNIQUES

Synthesis. All compounds were obtained from conproportionation reactions of stoichiometric ratios of $LaBr_3$, La (chempur, >99.9%), and Tn (Tn = Ru, Merck, > 99.9%, Ir, chempur, > 99.9%) in welded tantalum containers sealed under He and further encapsulated in evacuated fused-silica jackets. $LaBr_3$ was synthesized via the ammonium-halide-route and purified by sublimation.[19] Because of high sensitivity to air and moisture, all of the sample preparations were completed under a dry nitrogen atmosphere in a glovebox.

The samples were first heated to 1050 °C for one week and then slowly cooled to 700 °C at a rate of 1 °C/hour and rapidly cooled to room temperature at a rate of 90 °C/hour. The resulting products appeared as black powders containing small crystals. All of the samples were checked for purity by powder X-ray diffraction (PXRD) using the Guinier technique on a HUBER G670 diffractometer (Mo Kα; λ = 0.71073 Å). Detailed phase analyses of both samples revealed that the targeted compounds appeared as the major phase beside traces of unreacted $LaBr_3$. Under consideration of the detection limit of PXRD no further compounds, that is, impurities, could be identified (Supporting Information, Figure S1). In addition, the novel compositions $\{TnLa_3\}Br_3$ (Tn = Rh, Pt) were obtained as black powders in high yield from similar conproportionation reactions using the corresponding transition metals.

Structure Determination. To determine the structure of the products, single crystals selected from each reaction were transferred into 0.1 mm glass capillaries and sealed in a glovebox. Sets of single crystal X-ray diffraction (SCXRD) data were collected at room temperature on a STOE IPDS I diffractometer. The structures were solved using direct methods with SHELXS-97 and refined based on F^2.[20] The PLATON software package was used to check the symmetry of the compounds, while absorption corrections were carried out by the programs X-RED and X-SHAPE.[21,22] Selected crystallographic details, refinement parameters, atomic positions, and displacement parameters are listed in Tables 1 and 2.

Energy Dispersive X-ray (EDX) Analysis. Chunks of the compounds were selected from the bulk sample and prepared for measurement under a dry nitrogen atmosphere in a glovebox. A conductive carbon layer was added to the surface for the measurements. The samples were immediately transferred to a FEI Nova Nano Scanning Electron Microscope 430 that was equipped with an EDAX ApolloX EDX spectroscope. The samples were imaged using the secondary electrons as in the Supporting Information, Figure S4.

Table 1. Selected Crystallographic Data and Refinement Parameters for $\{TnLa_3\}Br_3$ (Tn = Ru, Ir)

	$\{RuLa_3\}Br_3$	$\{IrLa_3\}Br_3$
space group, Z	$I4_132$, (No. 214), 8	$I4_132$, (No. 214), 8
a (Å)	12.125(2)	12.174(2)
volume (Å^3)	1782.4(4)	1804.2(5)
F (000)	2560	2824
2θ range [deg]	2.38−28.08	4.10−27.96
index ranges	$-15 \le h \le 15$, $-16 \le k \le 15$, $-15 \le l \le 15$	$-16 \le h \le 15$, $-15 \le k \le 15$, $-14 \le l \le 14$
completeness	99.6%	99.6%
no of obs. refls.	8486	8462
no. ind. refls.	371 [R_{int} = 0.1523]	370 [R_{int} = 0.1386]
μ (Mo Kα; mm^{-1})	29.102	41.814
abs. corr.	numerical	numerical
GOF (F^2)	1.006	1.024
R_1, ωR_2 [$I_0 > 2\sigma(I)$]	0.0500; 0.1190	0.0292; 0.0654
R_1, ωR_2 (all data)	0.0782; 0.1282	0.0505; 0.0711

Table 2. Position and Equivalent Isotropic Displacement Parameters for $\{TnLa_3\}Br_3$ (Tn = Ru, Ir)[a]

atom	x	y	z	U [Å^2 × 10^3]
		$\{RuLa_3\}Br_3$		
Ru	1/8	1/8	1/8	0.0233 (7)
La	1/8	0.1109 (1)	0.3608 (1)	0.0284 (4)
Br	0.1330 (1)	3/8	0.3830 (1)	0.0323 (6)
		$\{IrLa_3\}Br_3$		
Ir	1/8	1/8	1/8	0.0126 (3)
La	1/8	0.1104 (7)	0.3610 (7)	0.0189 (3)
Br	0.1329 (1)	3/8	0.3829 (1)	0.0237 (4)

[a] U equals one third of the trace of the orthogonalized U^{ij} tensor.

Computational Details. Electronic structure calculations were performed using the tight-binding, linear muffin-tin orbital (TB-LMTO) method with the atomic sphere approximation (ASA) using the Stuttgart code.[23−25] Crystallographic data of the compounds studied were transformed to the TB-LMTO-ASA software package with the aid of the WXDragon program.[26] The radii of the Wigner-Seitz (WS) spheres were automatically generated and overlapping potentials were optimized to guarantee an optimal approximation of full potentials. The calculations also employed empty spheres in the voids with their positions and WS radii listed in the Supporting Information. The basis set utilized the following orbitals (down-folded[27] orbitals are in parentheses): Ir-6p/6s/5d/(5f); Ru-5p/5s/4d/(4f); La-6p/(6s)/5d/4f; Br-(5s)/4d/(4p); I-(6s)/5p/(5s)/(4d). The corresponding WS radii [Å] were: Ir, 2.99; Ru, 2.62−2.91; La, 3.00−3.75; Br, 3.18−3.62; and I, 3.56−3.85. The respective cubic $\{TnLa_3\}Br_3$ (Tn = Ru, Ir) and monoclinic $\{RuLa_3\}X_3$ (X = "Br", I) structures used 155 and 70 irreducible ***k***-points. Plots of the DOS and −COHP curves are shown below. A (chemical) bonding analysis was also completed based on the values of the integrated COHP (ICOHP) values.

To investigate and understand the structural preferences between the cubic and the monoclinic $\{TnLa_3\}X_3$ (X = Br, I) cases, calculations on hypothetical models of a monoclinic "$\{RuLa_3\}Br_3$" were performed with the Vienna ab initio simulation package (VASP).[28−31] VASP calculations were carried out using the projector augmented-wave (PAW) method of Blöchl and adapted in VASP by Kresse and Joubert.[32,33] The potentials for La, Br, and Ru are based, respectively, on [Kr4d], $4s^24p^5$ and $5s^14d^7$ electron configurations. Exchange and correlation was described by the Perdew−Burke−Ernzerhof 96

dx.doi.org/10.1021/ic300838a | Inorg. Chem. 2012, 51, 11356−11364

generalized gradient approximation (GGA-PBE).[34] A 2 × 6 × 2 Monkhorst-Pack *k*-points grid[35] was used to sample the first Brillouin zone for reciprocal space integrations. The energy cutoff of the plane wave basis set was 500 eV. Full structural optimizations, which included lattice parameters and atomic coordinates, were completed using VASP version 4.6 in a three-step process following program protocol.[28−31] With these settings the calculations converged to less than 1 meV/formula unit (f.u.).

III. RESULTS AND DISCUSSION

Structural Details. Two novel compounds with compositions $\{TnLa_3\}Br_3$ (Tn = Ru, Ir) were discovered using powder and single crystal X-ray diffraction. These structures are members of a cubic family with the general formulation $\{Tn_{1/4}R_{6/2}\}X_{9/3}Tn_{3/4}$ and crystallize in the space group $I4_132$ (No. 214) ($\{PtPr_3\}I_3$-type) with the Ca_3PI_3-type structure.[36] As shown in Table 1, lattice parameters and cell volume of the Ir containing compound are larger than for the corresponding Ru compound because of the increased effective atomic covalent radii from Ru (1.30 Å) to Ir (1.35 Å).[37] EDX analysis further confirmed the presence of the respective component elements (La, Ir, Br; or La, Ru, Br) and no other impurity elements. A semiquantitative analysis of the metal atom ratios suggests they are present in a ratio of 3:1:3. Furthermore, the analysis also indicated regions that contained only La and Br likely arising from the reactant $LaBr_3$.

The cubic structure type can be described as a defect NaCl-type structure by building a cubic close packing of Tn and X atoms with R atoms incorporated in 3/4 of all octahedral voids, in particular, those voids surrounding each Tn atom. More specifically, the compounds are composed of octahedral La clusters that are condensed via three common edges to construct quasi-infinite chains cycling around a 4_1-screw axis (Figure 1). The clusters are centered by Tn atoms sitting on Wyckoff site 8*a* ($^1/_8$,$^1/_8$,$^1/_8$) with site symmetry D_3. The $Br^{i\text{-}i\text{-}i}$ ligands cap nine edges of each cluster in a μ_2-type fashion, allowing their incorporation into the cluster network. The corners of all clusters are also connected via *exo*-Br ligands to the corners of neighboring units. As a result of the different edge-capping Tn and Br ligands, three different La−La distances are observed for each cluster. The La−La distances of the three Tn μ_2-capped edges are 3.8010(3) Å and 3.8230(2) Å for Ru and Ir, respectively, whereas the remaining nine edges that are μ_2-capped by $Br^{i\text{-}i\text{-}i}$ ligands show slightly longer bond distances. The Br−La distances are in good agreement with observed data of similar known compounds.[11]

On the contrary, the ruthenium-containing compound with the same general composition in the analogous iodine system, that is, $\{RuLa_3\}I_3$, has been previously reported to crystallize in a monoclinic structure ($\{RuPr_3\}I_3$-type, $P2_1/m$).[12,14] This structure also exhibits a cubic close packing of Tn and X atoms with 3/4 of all octahedral voids occupied by R atoms. In addition to the structural change from the cubic bromide, the monoclinic phase contains three independent La sites (Wyckoff's 2*e*, 2*e*, 2*e*), three halogen sites (Wyckoff's 2*e*, 2*e*, 2*e*), and one transition metal site (Wyckoff 2*e*). The structure of the monoclinic $\{TnR_3\}X_3$ can be described as bioctahedral chains of R clusters encapsulating transition metals.[12,14] It is worth noting that in contrast to the cubic $\{TnR_3\}X_3$ compositions, the monoclinic structure contains four edges of each $\{TnR_6\}$ unit that are μ_2-capped by the Tn, while the remaining 8 edges are μ_2-capped by X ligands (Figure 2). In addition, each chain is connected via *exo*-X bonds to neighboring chains.

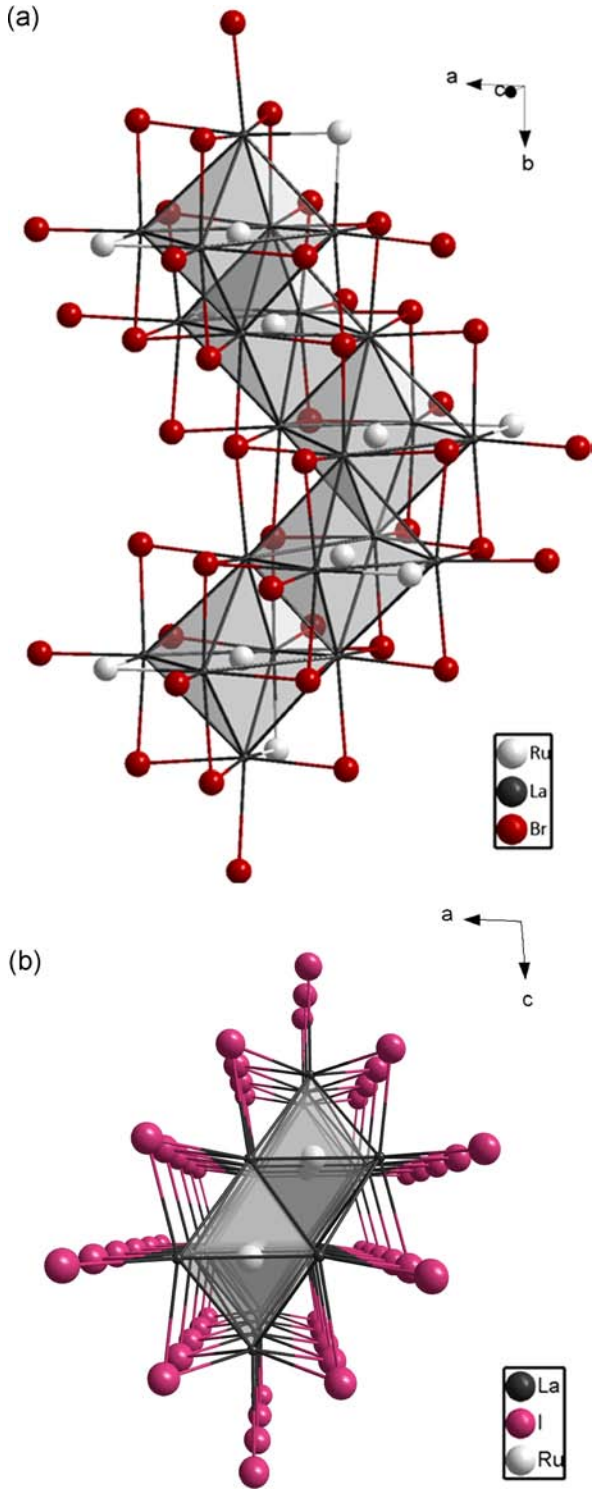

Figure 1. Representation of the (**a**) cubic $\{RuLa_3\}Br_3$-chain around a 4_1-screw axis and (**b**) the monoclinic bioctahedral $\{RuLa_3\}I_3$ chain.[12,14].

The cubic close packing of Tn and X atoms in the monoclinic and cubic structures both contain (nearly) planar close packed planes of transition metal and halogen atoms, which enclose the La atoms. In contrast to cubic $\{TnLa_3\}Br_3$ (Tn = Ru, Ir), where each close packed sheet is filled by 75% Br and 25% Tn atoms, the monoclinic $\{RuLa_3\}I_3$ structure has 50% of the close packed sheets occupied exclusively by I atoms (red lines, Figure 3). As a result, three different La coordination

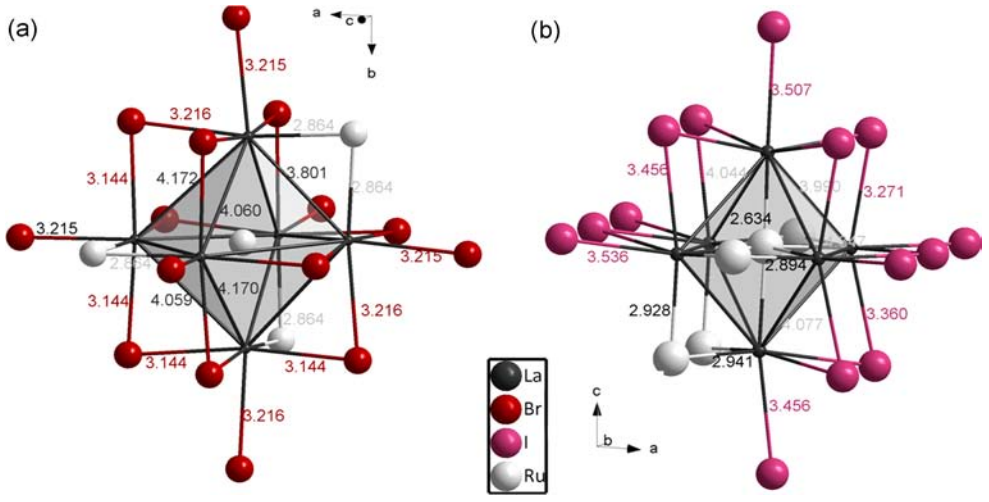

Figure 2. (a) $\{RuLa_6\}Br_{15}Ru_3$ and (b) $\{RuLa_6\}I_{14}Ru_4$ units from cubic $\{RuLa_3\}Br_3$ and monoclinic $\{RuLa_3\}I_3$, respectively, with selected interatomic distances.

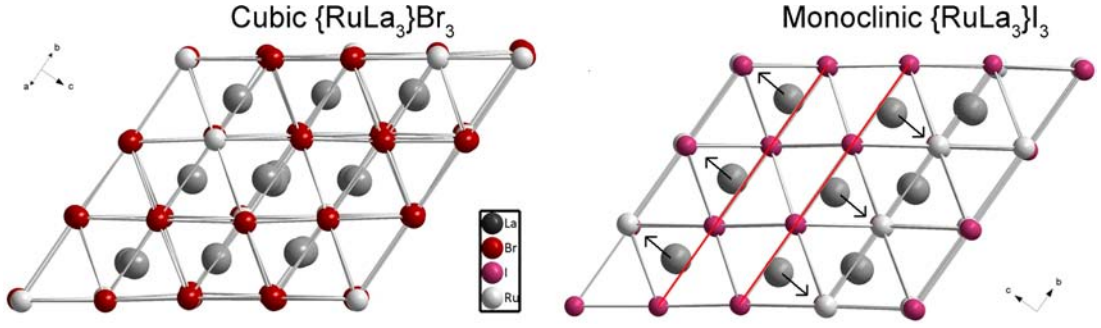

Figure 3. Close packed sheets of Ru and X (Br or I) atoms in $\{RuLa_3\}Br_3$ (left) and $\{RuLa_3\}I_3$. Ru (light gray) and X (Br: red, I: violet) build up ccp layers, La (dark gray) is situated in 3/4 of all the octahedral holes. Sheets which are exclusively filled by I are indicated (red lines).

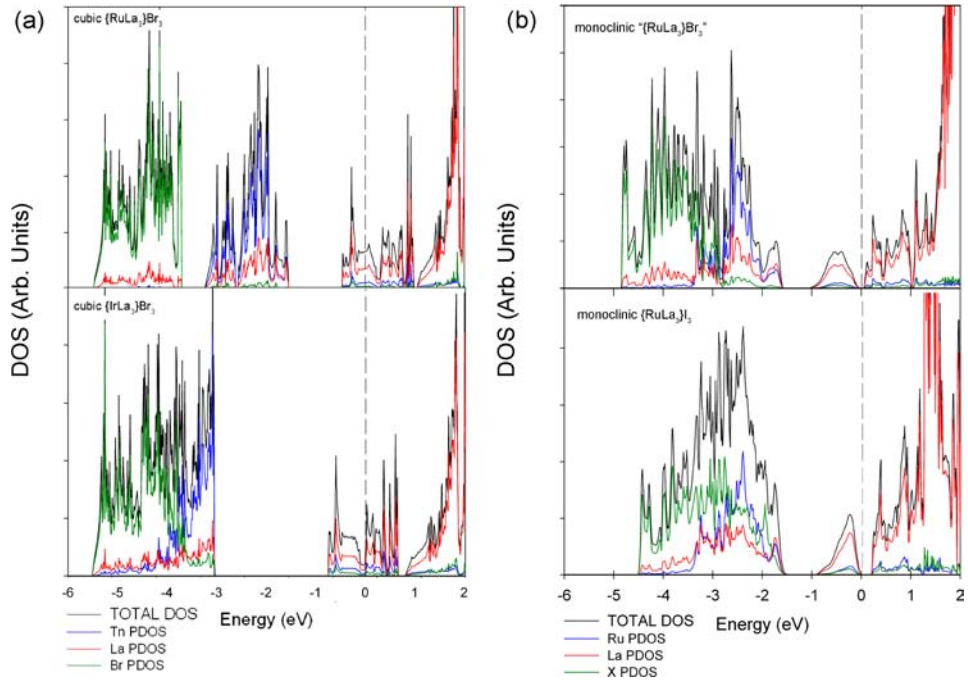

Figure 4. Partial DOS of (a-top) cubic $\{RuLa_3\}Br_3$, (a-bottom) cubic $\{IrLa_3\}Br_3$, (b-top) monoclinic "$\{RuLa_3\}Br_3$", and (b-bottom) monoclinic $\{RuLa_3\}I_3$.

dx.doi.org/10.1021/ic300838a | *Inorg. Chem.* 2012, 51, 11356−11364

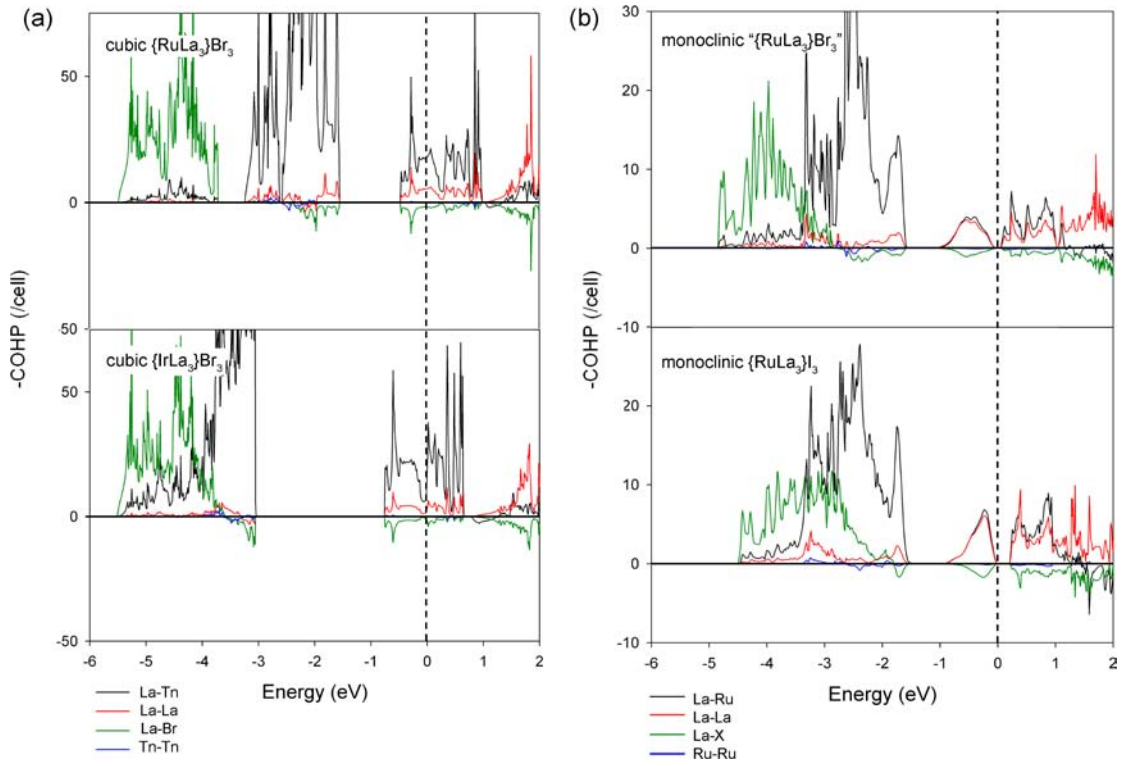

Figure 5. COHP curves of cubic $\{RuLa_3\}Br_3$ (a-top), cubic $\{IrLa_3\}Br_3$ (a-bottom), monoclinic "$\{RuLa_3\}Br_3$" (b-top), and monoclinic $\{RuLa_3\}I_3$ (b-bottom).

spheres are observed in monoclinic $\{RuLa_3\}I_3$: one La is coordinated by 3 I and 3 Ru; a second is coordinated by 4 I and 2 Ru; and, finally, a La is surrounded by 5 I and 1 Ru atom. Comparatively, the cubic $\{TnLa_3\}Br_3$ (Tn = Ru, Ir) compound contains only one La coordination sphere of 4 Br and 2 Ru atoms around the central La atom. Since the clusters in the monoclinic $\{RuLa_3\}I_3$ structure are encompassed by a large iodine sheath, the further condensation of La atoms into an agglomeration of clusters cannot be accomplished.[18]

A closer inspection of the close packed sheets in monoclinic $\{RuLa_3\}I_3$ shows that the La2 site, which is exclusively coordinated by 5 I atoms and 1 Ru atom, shifts from the center of the octahedral void that is formed by the closed pack layers toward the Ru atoms. As a result, a relatively short La−Ru distance of 2.634(1) Å is observed in contrast to an average La−Ru distance of 2.870 Å in monoclinic $\{RuLa_3\}I_3$.[14] This is in stark contrast to cubic $\{RuLa_3\}Br_3$ (Figure 3), which contains La atoms centered in the octahedral void.

Electronic Structure of the $\{TnR_3\}X_3$ Compounds. The first investigation of the electronic structure for interstitially centered rare earth cluster compounds ($\{TnR_6\}X_{12}R$ type) was based on EH calculations.[38] The theory exhibited Tn−R interactions similar to the bonding in *Werner* complexes.[7] Additionally, the band structures of several other compounds were analyzed by EH calculations and showed similar bonding features.[5,11,12,14,15,39−45] However, only a few examples of interstitially centered rare earth cluster compounds have been analyzed using density functional theory (DFT)-based calculations.[11,18,46−48]

Densities of States (DOS). A comparison of the DOS curves for the cubic compounds $\{RuLa_3\}Br_3$ and $\{IrLa_3\}Br_3$, shown in Figure 4a, indicates that the states near the Fermi level are composed primarily of the La 5d states for both compounds (partial DOS (PDOS) curves are presented in Supporting Information, Figure S5). Below E_F, there is a much wider gap (between −0.75 and −3.04 eV) in $\{IrLa_3\}Br_3$ relative to $\{RuLa_3\}Br_3$ (between −0.46 and −1.55 eV) because of the higher effective nuclear charge in Ir as a consequence of the lanthanide contraction. For instance, the Ru 4d states reside mostly between −1.54 and −3.24 eV while the Br states have moved below −3.71 eV. Moreover, the dispersion of the Ir 5d states is smaller than that for the Ru 4d states. Integrating the DOS curves in both cases reveals that there is one additional orbital per formula unit residing in the energy region near the Ru 4d or Ir 5d bands. This orbital is the totally symmetric (a_{1g}-type) octahedral cluster orbital,[38] which overlaps with the 5s atomic orbital (AO) of Ru or the 6s AO of Ir in its center. In addition, the DOS near E_F arise primarily from the t_{1u}-type octahedral cluster orbitals, which include small contributions from Ru 5p or Ir 6p AOs. These regions of the DOS contain 12 states per primitive unit cell, which contains 4 such $\{TnLa_6\}$ clusters. The condensation of these $\{TnLa_6\}$ clusters into mutually perpendicular spirals along each of the unit cell axes creates a pseudogap in this DOS region for valence electron counts of 32.0−33.7 VE.

Although the gross features of the DOS near the Fermi level are similar for the two cubic compositions, they differ in their respective valence electron (VE) counts. In particular, $\{RuLa_3\}Br_3$ contains 32 VEs whereas $\{IrLa_3\}Br_3$ has 33 VE. As a result, E_F in $\{RuLa_3\}Br_3$ falls on a local maximum in the DOS below the pseudogap, while E_F in $\{IrLa_3\}Br_3$ falls in the pseudogap. These different characteristics in the DOS indicate potentially different conductivity for $\{RuLa_3\}Br_3$, which should be metallic, and $\{IrLa_3\}Br_3$, which should be a poor metal.

In addition to the cubic $\{TnLa_3\}Br_3$ (Tn = Ru, Ir) type compounds, a hypothetical monoclinic "$\{RuLa_3\}Br_3$" structure

dx.doi.org/10.1021/ic300838a | *Inorg. Chem.* 2012, 51, 11356−11364

Table 3. Distances, −ICOHP/Bond, Number of Interactions, and Ave. −ICOHP for Cubic $\{TnLa_3\}Br_3$ (Tn = Ru, Ir)

	distances		−ICOHP/bond			ave. −ICOHP [eV/bond]	
interaction	$\{RuLa_3\}Br_3$	$\{IrLa_3\}Br_3$	$\{RuLa_3\}Br_3$	$\{IrLa_3\}Br_3$	no. of bonds	$\{RuLa_3\}Br_3$	$\{IrLa_3\}Br_3$
La−Tn	2.8647 (1)	2.8785 (9)	1.9092	1.8678	48	1.9092	1.8679
La−La 1	3.8010 (3)	3.8230 (2)	0.1725	0.1371	12		
La−La 2	4.0586 (2)	4.0779 (1)	0.0603	0.0488	24	0.0702	0.0580
La−La 3	4.1707 (9)	4.1891 (8)	0.0496	0.0428	48		
La−Br 1	3.1443 (2)	3.1548 (2)	0.4864	0.4354	48	0.4507	0.4047
La−Br 2	3.2155 (1)	3.2258 (1)	0.4150	0.3740	48		
Tn−Tn	4.2867 (4)	4.3040 (1)	0.0037	0.0043	12	0.0037	0.0043

was investigated. The hypothetical model was utilized to reveal structural preferences resulting from the band structures of the two competing structure types. The development of the structural model was completed by using the lattice parameters and atomic positions from the monoclinic $\{RuLa_3\}I_3$ as a starting point and employing VASP to perform structural optimizations, as described above. The electronic structure was then calculated using TB-LMTO-ASA and the optimized lattice parameters and atomic positions determined from VASP, provided in Supporting Information, Table S2.

The DOS of the monoclinic $\{RuLa_3\}X_3$ (X = "Br", I) exhibits a different electronic structure relative to the cubic compounds. The iodine 5p states are higher in energy than the Br 4p states because of the decreased electron affinity of Iodine, while the Ru 4d and La 5d states lie in the same range as in the cubic $\{RuLa_3\}Br_3$ compound. Additionally, in the hypothetical monoclinic "$\{RuLa_3\}Br_3$" the Br 4p states lie below the Ru 4d and La 5d states, respectively. Nevertheless, the bands located between −5 and about −1.5 eV in both figures account for the Br 4p, the Ru 4d, or Ir 5d, and the totally symmetric $\{TnLa_6\}$ cluster bonding orbital. A major difference in these DOS curves from those for the cubic structures occurs at the Fermi level, at which a gap opens between E_F and +0.05 eV for "$\{RuLa_3\}Br_3$" and E_F and +0.20 eV for $\{RuLa_3\}I_3$ rather than a pseudogap. Note that the gap is smaller in "$\{RuLa_3\}Br_3$" than in the corresponding iodine structure. This gap corresponds to a VE count of 32 valence electrons, suggesting "$\{RuLa_3\}Br_3$" as well as $\{RuLa_3\}I_3$ would be semiconductors; however, conductivity of the latter compound has not been measured to the best of our knowledge. This region of the DOS curves also may be assigned to the t_{1u}-type cluster orbitals of $\{TnLa_6\}$,[38] with some small contributions from Ru 5p or Ir 6p. The opening of the band gap arises from the connectivity of these clusters into condensed and distorted zigzag chains along the monoclinic *b*-axis.[12]

In summary, an analysis of the DOS curves for cubic $\{TnLa_3\}Br_3$ and monoclinic $\{TnLa_3\}X_3$ suggests that they gain significant stability from La−X and La−Tn bonding, and differentiate their structures through changes in their cluster condensation by occupation of one set of cluster bonding orbitals, namely, the t_{1u}-type orbitals. To investigate this outcome in more detail, we followed up with an analysis of COHP curves.

Bonding Analysis. In cubic $\{TnLa_3\}Br_3$ (Tn = Ru, Ir) and monoclinic $\{RuLa_3\}X_3$ (X = "Br", I), the various COHP curves, illustrated in Figure 5, and −ICOHP values, summarized in Tables 3 and 4, show modest La−La interactions and extensive La−Tn bonding interactions below E_F. Therefore, by considering the Tn as the central atom and La as the ligand these $\{TnLa_6\}$ clusters can be described as complexes in the anti-*Werner* sense.[7] Nevertheless, contributions from La−La bonding in the a_{1g}-type and t_{1u}-type cluster orbitals is evident.

Table 4. Ave. −ICOHP, No. of Bonds Per Cell, Cumulative −ICOHP Per Cell, and Contribution for Cubic $\{TnLa_3\}Br_3$ (Tn = Ru, Ir) and Monoclinic $\{RuLa_3\}X_3$ (X = "Br", I)[a]

	ave. −ICOHP [eV/bond]	no. of bonds per cell	cumulative −ICOHP per cell	contribution [%]
		Cubic $\{RuLa_3\}Br_3$		
La−Ru	1.9092	48	91.640	65.061
La−La	0.0702	84	5.901	4.189
La−Br	0.4507	96	43.268	30.719
Ru−Ru	0.0037	12	0.044	0.031
		Cubic $\{IrLa_3\}Br_3$		
La−Ir	1.8678	48	89.655	67.191
La−La	0.0580	84	4.872	3.652
La−Br	0.4047	96	38.854	29.119
Ir−Ir	0.0043	12	0.052	0.039
		Monoclinic "$\{RuLa_3\}Br_3$"[a]		
La−Ru	2.3737	12	28.4848	64.28
La−La	0.1843	22	4.0548	9.15
La−Br	0.4891	24	11.7395	26.49
Ru−Ru	−0.0080	4	−0.0321	0.08
		Monoclinic $\{RuLa_3\}I_3$[a]		
La−Ru	2.4488	12	29.3861	60.87
La−La	0.2168	22	4.7705	9.88
La−I	0.5877	24	14.1060	29.22
Ru−Ru	−0.0036	4	−0.0143	0.03

[a]Bond distances and numbers of contacts for each interaction as well as −ICOHP/bond for monoclinic $\{RuLa_3\}X_3$ (X = "Br", I) are listed in the Supporting Information, Tables S6 and S7.

A direct comparison of the −ICOHP values for the cubic and monoclinic $\{TnR_3\}X_3$-type structures cannot be made. This issue arises because the average electrostatic potential in each DFT-based calculation is set to an arbitrary "zero" energy, such that the relative position of "zero" can vary from system to system.[49,50] As a result, without a true reference energy (or "zero" energy) across all systems, it is inappropriate to strictly compare the −ICOHP values. Nevertheless, projecting the integrated values as a percentage of the total bonding capability in the structure, by evaluating −COHP values for all nearest neighbor interactions, has been shown to provide insight into bonding differences between different structure types.[18]

For the cubic $\{TnLa_3\}Br_3$ (Tn = Ru, Ir) systems, the La−La −ICOHP values range between 0.0496 and 0.1725 eV/bond for Ru and 0.0428 and 0.1371 eV/bond for Ir. These values contribute 4.18% and 3.65% to the total bonding of their respective structures. Such relatively minor interactions between these cluster atoms mean that the bonding network could be illustrated in *Werner*'s sense of coordination

dx.doi.org/10.1021/ic300838a | *Inorg. Chem.* 2012, 51, 11356−11364

Table 5. Compilation of $\{TnR_3\}X_3$-Type Structures (R = La, Pr; X = Cl, Br, I)[a]

No of VEs	32	33	34	35	32	33	34
Chlorides					$\{RuPr_3\}Cl_3$[15]		
Bromides	$\{RuLa_3\}Br$[*]	$\{RhLa_3\}Br$[*] $\{IrLa_3\}Br_3$[*]	$\{NiLa_3\}Br_3$[11] $\{PtLa_3\}Br$[*]		$\{RuPr_3\}Br_3$[10] $\{OsPr_3\}Br_3$[10]	$\{CoPr_3\}Br_3$[10] $\{RhPr_3\}Br_3$[10] $\{IrPr_3\}Br_3$[10]	$\{PtPr_3\}Br_3$[10]
Iodides	$\{RuLa_3\}I_3$[12] $\{OsLa_3\}I_3$[9]	$\{IrLa_3\}I_3$[9]	$\{PtLa_3\}I_3$[9]	$\{AuLa_3\}I_3$[43]	$\{RuPr_3\}I_3$[12] $\{OsPr_3\}I_3$[9,13]	$\{IrPr_3\}I_3$[9]	$\{PtPr_3\}I_3$[9]

[a]Compounds which form the undistorted monoclinic and cubic $\{TnR_3\}X_3$-type structures are highlighted red and dark blue, respectively. The orthorhombic and tetragonal $\{TnR_3\}X_3$-type structures ($\{RuPr_3\}Cl_3$,[15] $\{NiLa_3\}Br_3$[11]) are marked green and blue. [*]This work.

networks.[7] Nevertheless, Schäfer's and von Schnering's traditional way of "drawing lines" is still a useful guide to recognize cluster coordination networks even though La−La-bonding is a minor structural component.[51]

It is worth noting that the La−Ir interactions are mainly situated from −5.5 to −3.0 eV, while the La−Ru-bonding interactions range between −3.2 and −1.6 eV. These results are certainly caused by the lower effective charge of Ru relative to Ir. Furthermore, the La−Tn interactions contribute 65.1% (Tn = Ru) and 67.2% (Tn = Ir) to the total −ICOHP. Thus, the La−Tn interactions in $\{IrLa_3\}Br_3$ are slightly more effective than in $\{RuLa_3\}Br_3$.

The La−Br interactions cross from bonding to antibonding states at −3.59 eV for $\{IrLa_3\}Br_3$ and −2.89 eV for $\{RuLa_3\}Br_3$. The occupation of antibonding La−Br states at a relatively low energy is indicative of less bonding character relative to the La−Tn bonds, but also indicates that La−La bonding orbitals of the $\{TnLa_6\}$ cluster are occupied. Because the −ICOHP values tend to scale similarly to bond strength, in general, then as bond length increases, the magnitude of the −ICOHP values will decrease. For example, the Tn−Tn separations in these compounds are 4.2867(4) Å and 4.3040(1) Å for Tn = Ru and Ir and, thus, show negligible orbital overlap populations and −ICOHP values (Table 3).

Comparing the COHP curves of monoclinic "$\{RuLa_3\}Br_3$" and $\{RuLa_3\}I_3$ to the cubic $\{TnLa_3\}Br_3$ (Tn = Ru, Ir) structures, a different bonding situation is observed. For instance, the monoclinic structure contains significantly larger La−La bonding contributions (9.15% for "$\{RuLa_3\}Br_3$" and 9.88% for $\{RuLa_3\}I_3$) to the total −ICOHP values relative to the cubic structures. These large differences in bonding contributions stem from the distinct bonding environments. In cubic $\{RuLa_3\}Br_3$ only three edges of a cluster are μ_2-capped by Ru, while in monoclinic $\{RuLa_3\}I_3$ four edges are capped by Ru-atoms (Figure 2) resulting in a broader condensation of $\{RuLa_6\}$ units. Additionally, there are 10.5 La−La interactions in cubic $\{RuLa_3\}Br_3$ in contrast to 11 La−La interactions per formula unit in monoclinic $\{RuLa_3\}I_3$. As a result, the La−La contribution to the total −ICOHP values indicates more effective metal−metal interactions in monoclinic $\{RuLa_3\}I_3$ compared to cubic $\{RuLa_3\}Br_3$. For instance, the relatively strong and short La1−La1 bond (3.999(2) Å) in $\{RuLa_3\}I_3$ is exclusively capped by Ru atoms in a μ_2-fashion. On the basis of Pearson's electronegativities,[52] in which Ru (4.50) is less electronegative than iodine (6.76), less electron withdrawal from the La1−La1 contact by the bridging Ru ligand could be predicted. In this context, integration of the PDOS at each of the La sites revealed that La2, which is surrounded by 1 Ru and 5 I atoms, is the most electron-deficient ("oxidized") metal site. Simultaneously, one should recall that these La2 sites are shifted toward the Ru atoms leading to a relatively short distance of 2.634(1) Å[14] and a large −ICOHP of 3.65 eV/bond·mol. Since the magnitudes of −ICOHP values correlate well with bond length, the longer the bond length, the greater is the tendency toward smaller integrated overlap populations, as observed here (additional −ICOHP/interactions can be extracted from Supporting Information, Tables S6 and S7).

Structural Preference. Former considerations on the structural preferences of the $\{TnR_3\}X_3$-type structures revealed that effects leading to the formation of any one structure type are rather complex and subtle.[3,9,13] In this context, previous band structure investigations of the two monoclinic $\{TnR_3\}X_3$-type structures showed that different relative orbital energies in both types account for a lack of structural distortion of the bioctahedral chains in the $\{RuPr_3\}I_3$-type structure compared to the $\{IrY_3\}I_3$-type structure.[14,18] More specifically, in the $\{IrY_3\}I_3$-type structure, Tn and R orbital energies are close, leading to shorter Tn−Tn distances and an observed structural distortion. On the contrary, in the $\{RuPr_3\}I_3$-type structure, the relative Tn and R orbital energies are rather distinct resulting in more polar Tn−R bonding and repulsive Tn−Tn interactions. For comparison between the relatively dissimilar cubic $\{PtPr_3\}I_3$-type and monoclinic $\{RuPr_3\}I_3$-type structures, however, the effects determining the preferred structure appear to be even more complex.[3,13] Interestingly, to the best of our knowledge, the competition between these two structure types is just observed for group 8 Tn interstitials, whereas $\{TnR_3\}X_3$ compounds with a group 9 or 10 Tn as an endohedral atom tend to crystallize in the cubic structure type (Table 5).[9,10,12−14,43]

A comparison of the DOS of cubic $\{RuLa_3\}Br_3$ and a hypothetical monoclinic "$\{RuLa_3\}Br_3$" can provide some insights about the competition between the two structure types. In the case of cubic $\{RuLa_3\}Br_3$, E_F lies within a broad peak below a notable pseudogap in the DOS (see Figure 4a), which typically indicates an electronic instability. On the other hand, the Fermi level of monoclinic "$\{RuLa_3\}Br_3$" falls in a narrow gap of the DOS (Figure 4b). Based solely on considerations of the electronic structures, one would predict the monoclinic structure type with the gap at E_F to be favored. Yet, $\{RuLa_3\}Br_3$ adopts the cubic structure type rather than the monoclinic one. Interestingly, the analogous cubic $\{RuPr_3\}X_3$ (X = Br, I) systems[10,12,18] form the monoclinic structure, as expected by the electronic structure. Although calculations on $\{RuPr_3\}Br_3$ have not been reported, it is likely that Pr and La will have the same structural preferences because of similar features of their valence electronic states[53] and form the monoclinic structure, which is in agreement with experimental observations.[10] Additionally, the analogous Os-containing compound, that is, $\{OsPr_3\}I_3$, has been reported to crystallize

in both structure types[9,13] and, thus, demonstrates the complexity and electronic subtleties of the $\{TnR_3\}X_3$ system (Table 5). In $\{IrLa_3\}Br_3$, E_F is placed in the pseudogap indicating electronic stability. Further calculations on the I-containing compounds showed a similar situation providing justification for the formation of the cubic structures.[9]

COHP analyses of the DOS for all structure types revealed that large bonding contributions stem from the La−Tn and La−X interactions (see Table 4). Accordingly, these interactions, as well as the minor, but evident, La−La interactions, could be considered as the essential bonding network of these compounds by providing significant stabilization of the electronic energy. A comparison of the percentage contributions among the different interactions for cubic $\{RuLa_3\}Br_3$ and the hypothetical monoclinic "$\{RuLa_3\}Br_3$" illustrates that the "polar" La−Br interactions are more significant in cubic $\{RuLa_3\}Br_3$ than in the hypothetical monoclinic "$\{RuLa_3\}Br_3$". In return, La−La interactions in the monoclinic "$\{RuLa_3\}Br_3$" structure play a larger role than in the cubic $\{RuLa_3\}Br_3$ (see Table 4). In monoclinic $\{RuLa_3\}I_3$ the contributions of the La−La interactions are larger than in cubic $\{RuLa_3\}Br_3$; however, the La−Ru interactions have a smaller percentage contribution than in the cubic bromide. In all cases the La−Ru interactions could be considered as significant polar intermetallic bonding interactions in the sense of *Brewer*.[18] Thus, a major difference between the cubic and monoclinic structures is the occurrence of a larger percentage of La−La bonding contributions in the monoclinic structures, which, in turn, reduces the contributions of more polar bonding interactions. The differences in these interactions arise from the distinctive connectivity of the $\{RuLa_6\}$ clusters, that is, numbers of La−La interactions, which also adjusts the DOS for the different structure types. For the case bromides, the formation of polar La−Br interactions seems to be preferred and, accordingly, the cubic $\{RuLa_3\}Br_3$ is formed instead of the monoclinic "$\{RuLa_3\}Br_3$". Thus, any electronic instability associated with the peak at E_F in the DOS of cubic $\{RuLa_3\}Br_3$ is overcome by the stronger driving force to maximize overall bonding in the cubic structure rather than adopt the monoclinic form, which shows a gap at the Fermi level. It remains possible that cubic $\{RuLa_3\}Br_3$ may alleviate its predicted electronic instability by a structural distortion at low temperatures, akin to the tetragonal structure of $\{NiLa_3\}Br_3$,[11] but this prediction deserves further study. Thus, it can be concluded that the balance between La−La, La−Tn, and La-X interactions and the relative orbital energies of Tn, La, and X are the major features that dictate structure preference in the $\{TnR_3\}X_3$ systems. Even though the changes in the electronic structure among the different specific cases are subtle, the consequences control the formation of a given structure.

IV. CONCLUSIONS

Herein, we have reported a pair of new cubic compounds in the series $\{TnLa_3\}Br_3$ (Tn = Ru, Ir). These structures contain clusters of $\{TnLa_6\}$, which can be described as anti-*Werner* compounds. In addition to these new compositions, the electronic structures of these compounds were calculated based on the DOS and COHP curves. From the overlap interactions it is clear a majority of the bonding populations reside between the La−Tn contacts, but that the La−La interactions as well as valence electron count do contribute to the different cluster condensation patterns. In the investigation of their electronic structures, a pseudogap was identified at 33 VE. In the case of the cubic $\{IrLa_3\}Br_3$ this pseudogap falls right at the Fermi level, indicating electronic stability and providing justification for the adoption of the cubic $\{TnR_3\}X_3$-type structure. However, removing 1 VE from this system, forming cubic $\{RuLa_3\}Br_3$, places E_F at a peak in the DOS which is an electronically unfavorable situation. Consequently, a competition between the cubic and the electronically favorable monoclinic $\{TnR_3\}X_3$-type structure arises for group 8 Tn. A close inspection of the relative percentage contributions for cubic $\{RuLa_3\}Br_3$ as well as monoclinic $\{RuLa_3\}X_3$ (X = "Br", I) revealed that covalent La−La interactions are more significant in the monoclinic structures which, in turn, show smaller polar contributions, that is, Ru−La and La−X interactions (X = Br, I). Accordingly, the balance of the respective bond frequencies which stem from the distinctive connectivity of $\{RuLa_6\}$ clusters seems to play a subtle role as a structure determining force.

■ ASSOCIATED CONTENT

Supporting Information

CIFs of $\{TnLa_3\}Br_3$ (Tn = Ru, Ir), powder diffractions patterns of the samples, results of EDX analyses of $\{TnLa_3\}Br_3$ (Tn = Ru, Ir), lattice and atomic parameters of the hypothetical monoclinic "$\{RuLa_3\}Br_3$" composition, computational details, tables of WS radii and positions of empty spheres, PDOS depending on Composites and Orbitals. This material is available free of charge via the Internet at http://pubs.acs.org.

■ AUTHOR INFORMATION

Corresponding Author

*E-mail: gmiller@iastate.edu.

Notes

The authors declare no competing financial interest.

■ ACKNOWLEDGMENTS

This work was generously supported by Deutsche Forschungsgemeinschaft, Bonn (SFB 608 "Komplexe Übergangsmetallverbindungen mit Spin- und Ladungsfreiheitsgeraden und Unordnung") (S.S. and G.M.) as well as the National Science Foundation-Materials World Network (DMR-08-06507, J.B. and G.J.M.). The research was carried out at facilities of the Iowa State University and the University of Cologne. S.S. is grateful for a Chemiefonds Doktorandenstipendium by Fonds der Chemischen Industrie e.V., Frankfurt. The authors also acknowledge I. Pantenburg for SCXRD, H. Schumacher for PXRD, and A. E. Gad for EDX as well as SEM measurement.

■ REFERENCES

(1) Meyer, G. *Chem. Rev.* **1988**, *88*, 93−107.
(2) Simon, A. *Angew. Chem.* **1988**, *100*, 163−188.
(3) Corbett, J. D. *J. Alloys Compd.* **1995**, *229*, 10−23.
(4) Simon, A.; Mattausch, H. J.; Ryazanov, M.; Kremer, R. K. *Z. Anorg. Allg. Chem.* **2006**, *632*, 919−929.
(5) Corbett, J. D. *J. Alloys Compd.* **2006**, *418*, 1−20.
(6) Meyer, G. *Z. Anorg. Allg. Chem.* **2008**, *634*, 2729−2736.
(7) Werner, A. *Z. Anorg. Allg. Chem.* **1893**, *3*, 267−330.
(8) Pfeiffer, P. *Z. Anorg. Allg. Chem.* **1915**, *92*, 376−380; *Z. Anorg. Allg. Chem.* **1916**, *97*, 161−174.
(9) Payne, M. W.; Dorhout, P. K.; Corbett, J. D. *Inorg. Chem.* **1991**, *30*, 4960−4962.
(10) Llusar, R.; Corbett, J. D. *Inorg. Chem.* **1994**, *33*, 849−853.
(11) Zheng, C.; Mattausch, H. J.; Hoch, C.; Simon, A. *Z. Anorg. Allg. Chem.* **2009**, *635*, 2429−2433.

(12) Payne, M. W.; Dorhout, P. K.; Kim, S.-J.; Hughbanks, T. R.; Corbett, J. D. *Inorg. Chem.* **1992**, *31*, 1389−1394.
(13) Park, Y.; Martin, J. D.; Corbett, J. D. *J. Solid State Chem.* **1997**, *129*, 277−286.
(14) Köckerling, M.; Martin, J. D. *Inorg. Chem.* **2001**, *40*, 389−395.
(15) Herzmann, N.; Mudring, A.-V.; Meyer, G. *Inorg. Chem.* **2008**, *47*, 7954−7956.
(16) Larres, M., Meyer, G., private communication.
(17) Zheng, C.; Oeckler, O.; Mattausch, H. J.; Simon, A. *Z. Anorg. Allg. Chem.* **2001**, *627*, 2151−2162 , and lit. cited therein.
(18) Gupta, S.; Meyer, G.; Corbett, J. D. *Inorg. Chem.* **2010**, *49*, 9949−9957.
(19) Morss, L. R., Meyer, G. *Synthesis of Lanthanide and Actinide Compounds*; Kluwer Academic Publishers Press: Dordrecht, The Netherlands, 1991.
(20) Sheldrick, G. M. *SHELXS-97 and SHELXL-97, Programs for Crystal Structure Analysis*; University of Göttingen: Göttingen, Germany, 1997.
(21) Spek, A. L. *PLATON, a multipurpose crystallographic tool*; University of Utrecht: Utrech, The Netherlands, 1998.
(22) *X-SHAPE, Crystal Optimization for Numerical Absorption Correction (C)*, 1.06 ed.; Stoe & Cie GmbH: Darmstadt, Germany, 1999. *X-Area* , 1.16 ed.; Stoe & Cie GmbH: Darmstadt, Germany, 2003. *X-RED 1.22 ed., Stoe Data Reduction Program (C)*; Stoe & Cie GmbH: Darmstadt, Germany, 2001.
(23) Andersen, O. K. *Phys. Rev. B* **1975**, *12*, 3060.
(24) Andersen, O. K.; Jepsen, O. *Phys. Rev. Lett.* **1984**, *53*, 2571.
(25) Krier, G., Jepsen, O., Burkhardt, A., Andersen, O. K. *TB-LMTO-ASA Program*, 4.7 ed.; Max-Planck-Institut für Festkörperforschung: Stuttgart, Germany, 1995.
(26) Eck, B. *WXDragon*, 1.7.2; RWTH Aachen: Aachen, Germany, 2011.
(27) Lambrecht, W. R. L.; Andersen, O. K. *Phys. Rev. B* **1986**, *34*, 2439.
(28) Kresse, G.; Marsman, M.; Furthmüller, J. *Vienna Ab-initio Simulation Package (VASP): VASP, the GUIDE*; 2010
(29) Kresse, G.; Furthmüller, J. *J. Comput. Mat. Sci.* **1996**, *6*, 15.
(30) Kresse, G.; Furthmüller, J. *Phys. Rev. B.* **1996**, *54*, 11169.
(31) Kresse, G.; Hafner, J. *Phys. Rev. B.* **1993**, *47*, 558.
(32) Blöchel, P. E. *Phys. Rev. B* **1994**, *50*, 17953.
(33) Kresse, G.; Joubert, D. *Phys. Rev. B* **1999**, *59*, 1758.
(34) Pedrew, J. P.; Burke, K.; Ernzerhof, M. *Phys. Rev. Lett.* **1996**, *77*, 3865.
(35) Monkhorst, H. J.; Pack, J. D. *Phys. Rev. B* **1976**, *13*, 5188.
(36) Hamon, C.; Marchiand, R.; Laurent, Y.; Lang, J. *Bull. Soc. Fr. Miner. Crist.* **1974**, *97*, 6.
(37) Slater, J. C. *J. Chem. Phys.* **1964**, *41*, 3199.
(38) Hughbanks, T.; Rosenthal, G.; Corbett, J. D. *J. Am. Chem. Soc.* **1986**, *108*, 8289−8290.
(39) Brühmann, M.; Mudring, A.-V.; Valldor, M.; Meyer, G. *Eur. J. Inorg. Chem.* **2011**, 4083−4088.
(40) Lulei, M.; Martin, J. D.; Hoistad, L. M.; Corbett, J. D. *J. Am. Chem. Soc.* **1997**, *119*, 513−520.
(41) Uma, S.; Martin, J. D.; Corbett, J. D. *Inorg. Chem.* **1999**, *38*, 3825−3830.
(42) Payne, M. W.; Dorhout, P. K.; Corbett, J. D. *Inorg. Chem.* **1991**, *30*, 1467−1472.
(43) Mattausch, H. J.; Zheng, C.; Kienle, L.; Simon, A. *Z. Anorg. Allg. Chem.* **2004**, *630*, 2367−2372.
(44) Steinwand, S. J.; Corbett, J. D.; Martin, J. D. *Inorg. Chem.* **1997**, *36*, 6413−6422.
(45) Zheng, C.; Hoch, C.; Mattausch, H. J.; Simon, A. *J. Solid State Chem.* **2009**, *182*, 2307−2311.
(46) Zimmermann, S.; Brühmann, M.; Casper, F.; Heyer, O.; Lorenz, T.; Felser, C.; Mudring, A.-V.; Meyer, G. *Eur. J. Inorg. Chem.* **2010**, 2613−2619.
(47) Zheng, C.; Mattausch, H. J.; Hoch, C.; Simon, A. *Inorg. Chem.* **2008**, *47*, 2356−2361.
(48) Sweet, L. E.; Roy, L. E.; Meng, F.; Hughbanks, T. *J. Am. Chem. Soc.* **2006**, *128*, 10193−10201.
(49) Dronskowski, R.; Blöchel, P. E. *J. Phys. Chem.* **1993**, *97*, 8617−8624.
(50) Börnsen, N.; Meyer, B.; Grotheer, O.; Fähnle, M. *J. Phys.: Condens. Matter* **1999**, *11*, L 287.
(51) Schäfer, H.; von Schnering, H. G. *Angew. Chem.* **1964**, *76*, 833−868.
(52) Pearson, R. G. *Inorg. Chem.* **1988**, *27*, 734−740.
(53) Cotton, S. *Lanthanide and Actinide Chemistry*; John Wiley & Sons Ltd: Chichester, England, 2007.